Identification of an essential endogenous regulator of blood–brain barrier integrity, and its pathological and therapeutic implications

Enrico Cristante[a,1], Simon McArthur[a,1], Claudio Mauro[a], Elisa Maggioli[a], Ignacio A. Romero[b], Marzena Wylezinska-Arridge[c], Pierre O. Couraud[d], Jordi Lopez-Tremoleda[c], Helen C. Christian[e], Babette B. Weksler[f], Andrea Malaspina[g,h], and Egle Solito[a,2]

[a]William Harvey Research Institute, Barts and the London School of Medicine and Dentistry, Queen Mary University of London, London EC1M 6BQ, United Kingdom; [b]Department of Life Sciences, The Open University, Milton Keynes MK7 6AA, United Kingdom; [c]Institute of Clinical Science, Imperial College London, London W12 0NN, United Kingdom; [d]INSERM U1016, Institut Cochin, Université Paris Descartes, 75014 Paris, France; [e]Department of Physiology, Anatomy and Genetics, University of Oxford, Oxford OX1 3QX, United Kingdom; [f]Division of Haematology and Medical Oncology, Weill Medical College of Cornell University, New York, NY 10065; and [g]North-East London and Essex MND Care and Research Centre and [h]Centre for Neuroscience and Trauma, Blizard Institute, Queen Mary University of London, London E1 2AT, United Kingdom

This Feature Article is part of a series identified by the Editorial Board as reporting findings of exceptional significance.

Edited by Bruce S. McEwen, The Rockefeller University, New York, NY, and approved November 26, 2012 (received for review June 4, 2012)

The blood–brain barrier (BBB), a critical guardian of communication between the periphery and the brain, is frequently compromised in neurological diseases such as multiple sclerosis (MS), resulting in the inappropriate passage of molecules and leukocytes into the brain. Here we show that the glucocorticoid anti-inflammatory messenger annexin A1 (ANXA1) is expressed in brain microvascular endothelial cells, where it regulates BBB integrity. In particular, ANXA1$^{-/-}$ mice exhibit significantly increased BBB permeability as a result of disrupted interendothelial cell tight junctions, essentially related to changes in the actin cytoskeleton, which stabilizes tight and adherens junctions. This situation is reminiscent of early MS pathology, a relationship confirmed by our detection of a selective loss of ANXA1 in the plasma and cerebrovascular endothelium of patients with MS. Importantly, this loss is swiftly restored by i.v. administration of human recombinant ANXA1. Analysis in vitro confirms that treatment of cerebrovascular endothelial cells with recombinant ANXA1 restores cell polarity, cytoskeleton integrity, and paracellular permeability through inhibition of the small G protein RhoA. We thus propose ANXA1 as a critical physiological regulator of BBB integrity and suggest it may have utility in the treatment of MS, correcting BBB function and hence ameliorating disease.

The presence of narrow and dense tight junctions between adjacent endothelial cells is peculiar to the cerebral vasculature, and their integrity is essential for the maintenance of correct blood–brain barrier (BBB) function as the primary regulator of cross-talk between the brain and the rest of the body (1). Increasing evidence indicates that the integrity of this structural and functional barrier is compromised in neurological conditions such as multiple sclerosis (MS), Alzheimer's, and Parkinson diseases, leading to the failure of the normal mechanisms controlling passage of substances into the brain (2) and to the sensitization and/or worsening of pathologic conditions. Pharmacological intervention to prevent or correct BBB alteration in such diseases is a difficult task, but potential therapeutic leads can be gained from the study of endogenous mediators regulating barrier integrity.

Annexin A1 (ANXA1) is an important anti-inflammatory protein, principally known as a regulator of peripheral leukocyte migration and a promoter of macrophage phagocytosis (3). ANXA1 is expressed in several cell types within the brain, including ependyma and microglia, but in particular in the endothelium of the brain microvasculature (4), although its role in these cells remains obscure. We have previously shown glucocorticoids to up-regulate expression of ANXA1 in the cerebral endothelium (5), and, given that glucocorticoids enhance BBB tightness (6), we hypothesized that ANXA1 may play a role in the regulation of BBB permeability. Through combined in vitro and in vivo approaches, we have identified a dual role for ANXA1 in organizing the interendothelial cell tight and adherens junctions: (*i*) endogenously through its interactions with the actin cytoskeleton, and (*ii*) exogenously in an autocrine/paracrine via formyl peptide receptor 2 (FPR2), leading to the down-regulation of RhoA GTPase activity. Together, these two actions of ANXA1 regulate paracellular permeability in the BBB, and provide a major contribution to BBB integrity and function. Moreover, we describe a selective down-regulation of ANXA1 expression in the plasma and cerebral microvascular endothelia of patients with MS, strongly suggesting an explanation for the BBB dysfunction that is a typical early sign of this disease. All these findings pinpoint ANXA1 as a critical component of the BBB endothelium contributing to barrier integrity. Its autoparacrine role and the loss in patients with MS highlight the potential utility of the protein or its peptidomimetics as a therapeutic target for pathologic processes characterized by compromised BBB function, such as MS.

Results

AnxA1$^{-/-}$ Mice Show Constitutively Elevated BBB Permeability. As ANXA1 expression is modulated by steroids in the brain microvascular endothelium (5), we examined the effect of its deletion in AnxA1$^{-/-}$ mice in vivo through assessment of endothelial permeability by using a range of different approaches, namely MRI, transendothelial transport of Evans blue-labeled albumin, and extravasation of serum IgG.

Comparison of MRI signals from adult male WT and AnxA1$^{-/-}$ mice following i.v. administration of dimeglumine gadopentetate tracer (0.5 mM, 100 μL) revealed considerable leakage of contrast medium into the brain parenchyma in AnxA1$^{-/-}$ animals, whereas no changes before and after contrast agent administration were observed in WT littermate controls (Fig. 1*A*). Similarly, following i.v. injection of Evans blue dye, spectrophotometric analysis of brain dye content revealed significantly greater leakage in KO animals than their WT counterparts (Fig. 1*B*). The enhanced BBB

Author contributions: E.S. designed research; E.C., S.M., C.M., E.M., M.W.-A., J.L.-T., H.C.C., and E.S. performed research; I.A.R., P.O.C., B.B.W., A.M., and E.S. contributed new reagents/analytic tools; E.C., S.M., and E.S. analyzed data; and S.M. and E.S. wrote the paper.

The authors declare no conflict of interest.

This article is a PNAS Direct Submission.

[1]E.C. and S.M. contributed equally to this work.

[2]To whom correspondence should be addressed. E-mail: e.solito@qmul.ac.uk.

This article contains supporting information online at www.pnas.org/lookup/suppl/doi:10.1073/pnas.1209362110/-/DCSupplemental.

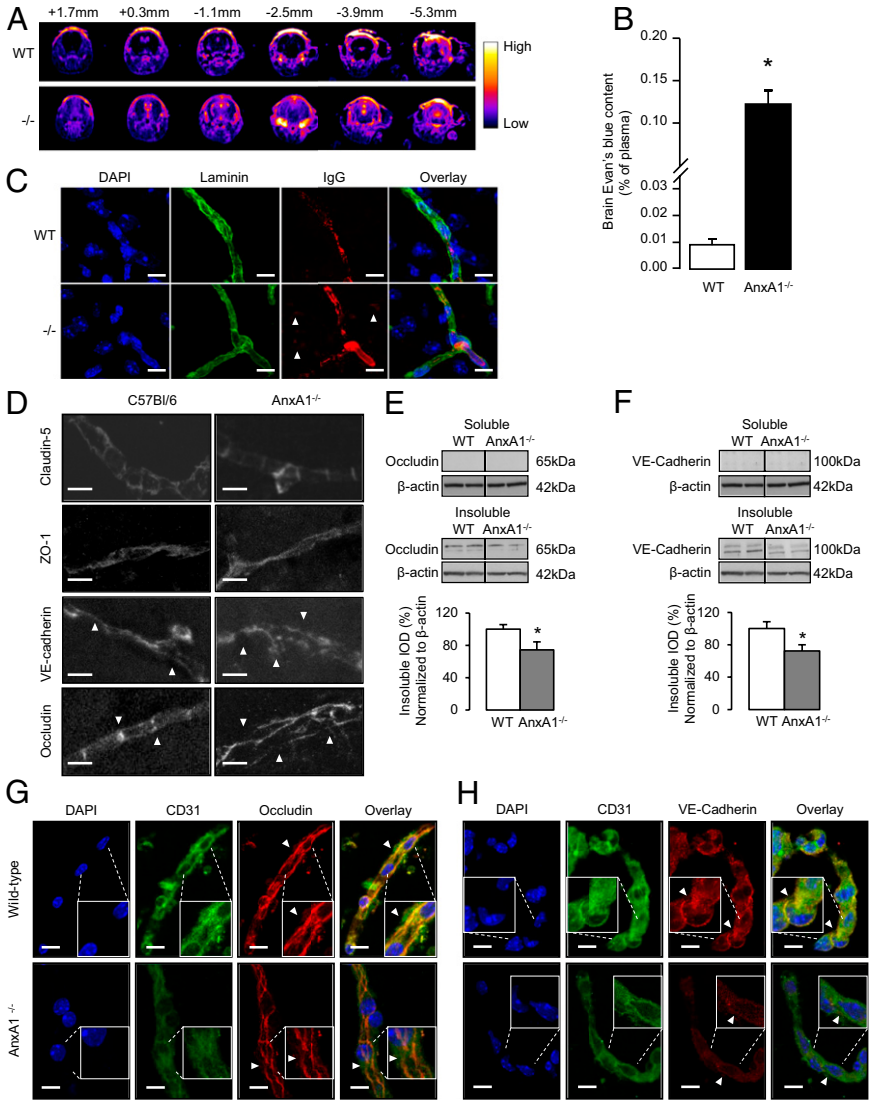

Fig. 1. BBB permeability is constitutively raised in AnxA1$^{-/-}$ mice. (*A*) T1-weighted dynamic contrast MRI series of coronal cranial sections taken at various distances from bregma of WT and AnxA1$^{-/-}$ mice. Brighter areas show increased dimeglumine gadopentetate leakage. Typical profile with $n = 5$ mice per genotype. (*B*) In vivo assessment of BBB paracellular permeability via Evans blue dye extravasation. Evans blue (100 μL 2% solution) was injected i.v. into WT or AnxA1$^{-/-}$ mice ($n = 6$) and allowed to circulate for 1 h. Brain dye content was then assessed spectrophotometrically and normalized to plasma levels. Data are means ± SEM (*$P <$ 0.05 vs. WT). (*C*) Extravasation of IgG into brain parenchyma in WT and AnxA1$^{-/-}$ mice. Tissue nuclei are stained with DAPI (blue), laminin (green) staining delineates the basement membrane of capillaries, and arrows indicate points of mouse IgG (red) distant from the blood vessels. (Scale bar: 10 μm.) (*D*) Immunofluorescent analysis of claudin-5, ZO-1, occludin, and VE-cadherin in cortical sections (20 μm) from WT and AnxA1$^{-/-}$ mice reveal disordered localization of occludin and VE-cadherin, but not claudin-5 or ZO-1; typical images from $n = 6$ mice per genotype. (Scale bar: 10 μm.) (*E* and *F*) Typical Western blot analysis of soluble and insoluble occludin (*E*) and VE-cadherin (*F*) content in cortical extracts from WT and AnxA1$^{-/-}$ mice, alongside β-actin loading controls. Histograms indicate densitometric analysis of blots, expressed as mean ± SEM ($n = 3$ independent experiments, each with $n = 4$ male samples/genotype; *$P <$ 0.05 vs. WT). (*G* and *H*) Confocal microscopic analysis of occludin (*G*) and VE-cadherin (*H*) expression in isolated cortical capillaries from WT and AnxA1$^{-/-}$ mice in vitro. Nuclei are labeled with DAPI, endothelial cells were identified by immunofluorescent detection of CD31 (green), and occludin and VE-cadherin are immunofluorescently labeled in red (typical images from $n = 3$ independent preparations; 511-nm optical sections. (Scale bar: 10 μm.)

permeability was confirmed immunohistochemically: AnxA1$^{-/-}$ mice exhibited IgG extravasation in the brain parenchymal whereas no IgG deposits were observed in WT littermates (Fig. 1*C*).

Expression and Distribution of Tight and Adherens Junction Proteins Are Disrupted in AnxA1$^{-/-}$ Mice. As barrier integrity is almost exclusively mediated by the tight and adherens junctions, we tested the hypothesis that the absence of ANXA1 could disrupt/perturb them. We investigated the distribution of the key tight junction molecule occludin and the adherens junction component vascular endothelial (VE)-cadherin by confocal microscopy. Both proteins revealed significant organizational disruption in AnxA1$^{-/-}$ mice (Fig. 1*D*), although similar disruptions were not seen in the tight junction molecules claudin-5 or zona occludens-1 (Fig. S1*A* and *B*), nor were alterations seen in the expression of the p-glycoprotein transporter MDR-1a (Fig. S1*C*) or other cellular and macromolecular components of the BBB, such as astrocytic end-feet, pericytes, or the basal lamina (Fig. S1*D*). Notably, histological analysis of kidney cortex, an unrelated tissue rich in tight junctions, revealed no evident occludin disorganization in AnxA1$^{-/-}$ mice compared with WT animals (Fig. S1*E*), supporting the endothelium-specific nature of these differences. Further analysis by Western blot revealed a significant reduction in occludin and VE-cadherin content in the insoluble, membrane-associated fraction of cortical homogenates in AnxA1$^{-/-}$ mice (Fig. 1 *E* and *F*). These data were confirmed by analysis of cerebral microvascular capillaries in vitro, in which disrupted organization and expression of occludin and VE-cadherin were apparent in vessels from AnxA1$^{-/-}$ mice compared with those from WT counterparts (Fig. 1 *G* and *H*). Importantly, as ANXA1 is a member of a large family of mammalian annexins (7) we examined possible compensatory changes in the closely related annexins A2 and A5 in isolated mouse brain vessels. No changes were apparent in expression of annexin A5, but there appeared to be an up-regulation in annexin A2 expression (Fig. S2), suggesting that, although compensation may have occurred, this is not sufficient to restore the loss of BBB function seen upon deletion of ANXA1.

ANXA1 Regulates Paracellular Permeability in an in Vitro Model of BBB. To examine the mechanisms underlying the increased BBB permeability and disrupted interendothelial junctions seen in AnxA1$^{-/-}$ mice, we used the human immortalized brain endothelial cell line hCMEC/D3 (8), a powerful tool widely used to investigate BBB physiology (9). We created stable clonal lines of these cells bearing full-length ANXA1 (FL) or an antisense sequence to ANXA1 (AS) (10) (Fig. S3 and Table 1), and characterized their barrier characteristics in tissue culture. By using a well-established method to examine the paracellular permeability of a monolayer of cells (11), we showed that AS clones had

Table 1. hCMEC/D3 clones release different amounts of ANXA1 into the cell culture medium

Clone	ANXA1/Released concentration, ng/mL
Mock transfected E3	4.563 ± 0.095
Antisense 4	3.33 ± 0.186*
Full length 11	5.820 ± 0.427*

Values presented as mean ± SEM.
*$P < 0.05$ vs. mock-transfected cells.

significantly greater transendothelial permeability than untransfected hCMEC/D3 cells, stable clones transfected with an empty pRc/CMV plasmid, or FL clones (Fig. 2*A*), primarily because of changes in paracellular rather than transcellular permeability. (No significant endocytosis of the fluorescent dextran used was detected, as shown in Fig. S4.) This finding was supported by studies showing the same AS cells to have significantly reduced transendothelial electrical resistance (Fig. 2*B*) compared with the other cell lines, and, moreover, FL cells exhibited paracellular permeability even lower than that of the untransfected hCMEC/D3 cells (Fig. 2*A*).

The contribution of ANXA1 toward endothelial tightness was confirmed by experiments in which administration of a neutralizing monoclonal antibody raised against ANXA1, but not an irrelevant IgG control, significantly enhanced paracellular permeability (Fig. 2*C*) in untransfected hCMEC/D3 cells.

ANXA1 Paracellular Permeability Is Mediated by an Interaction with Actin Cytoskeleton. Paracellular permeability across the cerebral microvascular wall is controlled by the presence of tight and adherens junction complexes between endothelial cells (1), structures we have shown to be markedly disrupted in the AnxA1$^{-/-}$ mice. Therefore, we first examined by EM the distribution of ANXA1 within hCMEC/D3 cells grown as a polarized monolayer. This analysis revealed that the protein is localized in the proximity of the cell membrane, and, most notably, is highly concentrated at points of close cell–cell contact (Fig. 2*D*). As such points of close contact between endothelial cells are the primary locations of tight and adherens junctions, we examined the expression of tight and adherens junction proteins in our FL and AS hCMEC/D3 clonal lines, finding a significant down-regulation in expression of occludin and VE-cadherin in AS cells (Fig. S2), and, more importantly, a clear loss in the normal peripheral organization of occludin and VE-cadherin in AS cells (Fig. 2*E*).

The stability of tight and adherens junctions within the intercellular connections is determined to a large extent by the actin cytoskeleton, and in particular by interactions between the actin cytoskeleton and the cell membrane (12). Hence, we examined the distribution of fibrillar actin within WT, FL, and AS hCMEC/D3 cells. Whereas WT and FL cells showed strong cortical actin staining, accompanied by the presence of clear stress fibers running parallel to the longitudinal axis of the cell, AS cells exhibited a distorted actin cytoskeleton, with a striking reduction in stress fibers, a marked alteration in cell shape and an apparent loss in polarity (Fig. 3*A*).

Given the profound changes seen in the actin cytoskeleton and loss of polarity of AS hCMEC/D3 clones, we investigated an association between ANXA1 and the actin cytoskeleton. Initial coimmunoprecipitation experiments identified a clear biochemical interaction between ANXA1 and β-actin (Fig. 3*B*); this evidence was supported through examination of points of ANXA1–β-actin binding in WT hCMEC/D3 cells by using confocal microscopy and a proximity ligation assay (Duolink; Olink Bioscience;

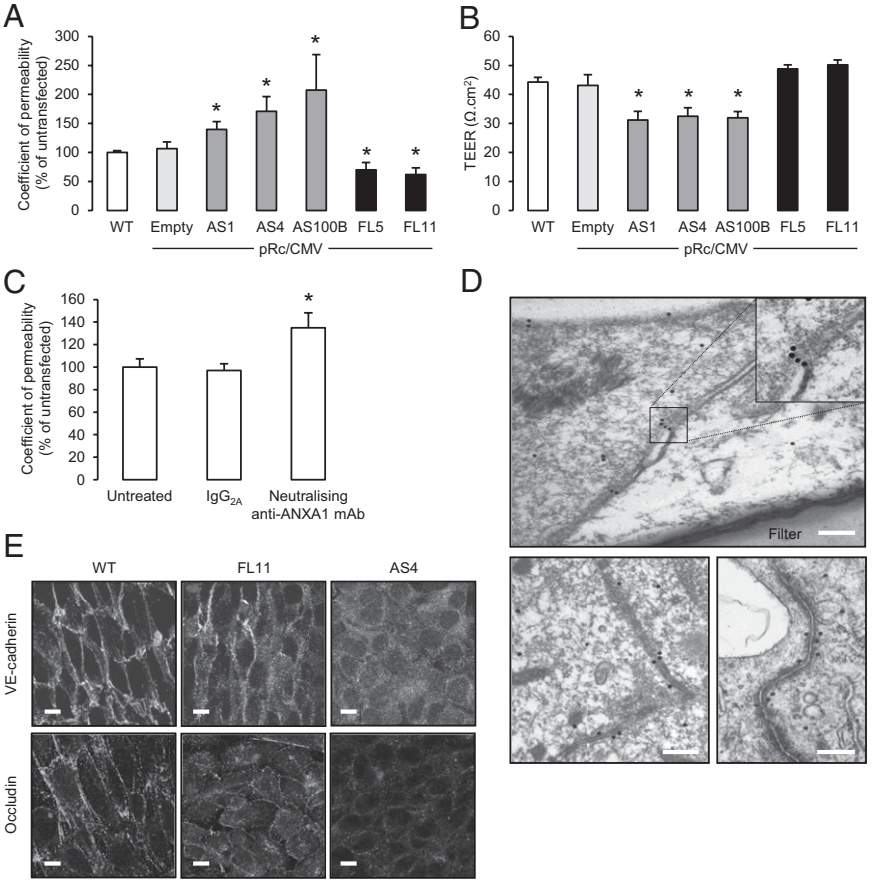

Fig. 2. ANXA1 expression modulates in vitro paracellular permeability. (*A* and *B*) Paracellular permeability coefficients (*A*) and transendothelial resistance (TEER; *B*) measured in WT hCMEC/D3 human brain microvascular endothelial cells or stable hCMEC/D3 clones transfected with a pRc/CMV plasmid alone (empty) or containing an antisense ANXA1 sequence (AS1, AS4, AS100B) or full-length ANXA1 (FL5, FL11); data are representative of at least three independent experiments, performed in triplicate, expressed as mean ± SEM (*$P < 0.05$ vs. WT clones). (*C*) Paracellular permeability of WT hCMEC/D3 monolayers following exposure to a neutralizing anti-ANXA1 antibody at 20 μg/mL for 3 h, compared with exposure to an irrelevant mouse IgG isotype control (30 μg/mL); data are representative of at least three independent experiments, performed in triplicate, expressed as mean ± SEM (*$P < 0.05$). (*D*) EM analysis of Immunogold labeling for ANXA1 in WT hCMEC/D3 cells grown as a polarized monolayer on a transwell polycarbonate filter reveals a striking localization of the protein at points of cell-cell contact. *Upper*: Transverse image through the cell monolayer. *Lower*: Vertical images of cell contacts. (Scale bar: 200 nm.) (*E*) Confocal microscopic analysis of VE-cadherin and occludin in polarized monolayers of WT, FL11, and AS4 hCMEC/D3 clones reveals marked disturbances in both proteins in AS clones (typical example from $n = 3$ independent preparations). (Scale bar: 10 μm.)

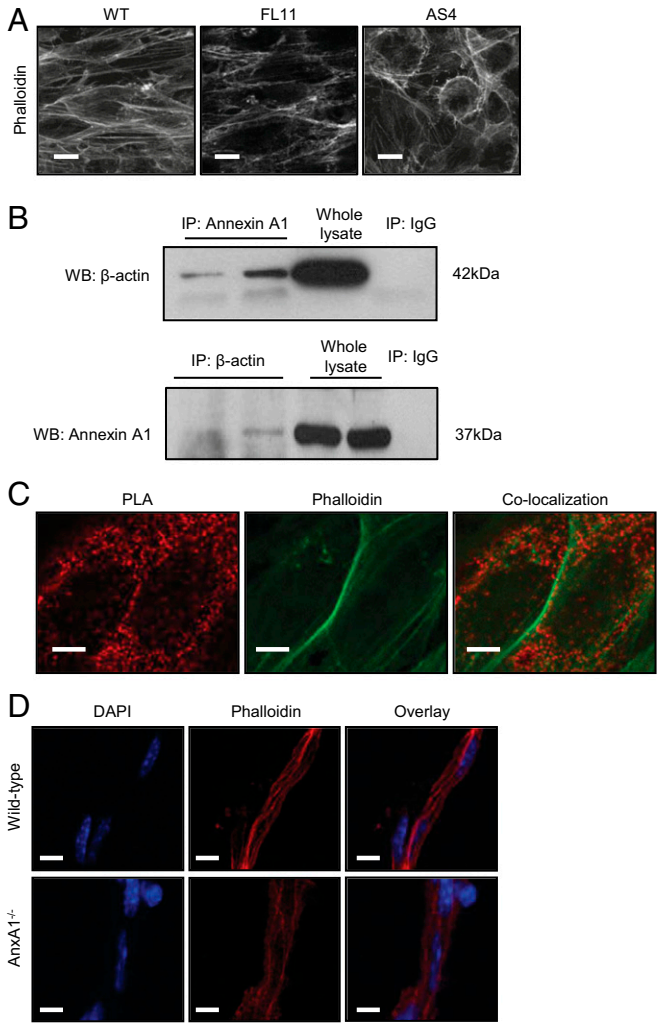

Fig. 3. ANXA1 regulates tightness through an interaction with the actin cytoskeleton. (*A*) Rhodamine-phalloidin staining of F-actin in WT, FL11, and AS4 hCMEC/D3 clones reveals a disorganized cytoskeletal structure in AS4 cells. (Scale bar: 10 μm.) (*B*) Coimmunoprecipitation analysis of ANXA1 and β-actin interaction: *Upper*: Total cell extracts (250 μg) were immunoprecipitated with 5 μg of a monoclonal anti–β-actin antibody, and Western blot was performed with anti-ANXA1 antibody. *Lower*: Cellular extracts were immunoprecipitated with 5 μg of an anti-ANXA1 antibody, and Western blot was performed with an anti–β-actin antibody. (*C*) Confocal microscopic analysis of ANXA1 and β-actin colocalization determined by use of the proximity ligation assay (PLA; red), and F-actin identified by rhodamine-phalloidin staining (green) in WT hCMEC/D3 cells. Images are from a 400-nm optical section. (Scale bar: 5 μm.) (*D*) Confocal microscopic analysis of the actin cytoskeleton in isolated brain capillaries from WT and AnxA1$^{-/-}$ mice, identified by staining nuclei with DAPI (blue) and F-actin with rhodamine-phalloidin (red; typical images from $n = 3$ independent preparations). (Scale bar: 10 μm.)

Fig. 3*C*). This technique, which identifies spatial points in which ANXA1 and β-actin are found within 40 nm of each other (13), revealed clear colocalization of ANXA1 and cytosolic G-actin (Fig. 3*C*). However, dense points of ANXA1–β-actin colocalization were also apparent alongside cortical F-actin fibrils, as defined by rhodamine-phalloidin binding, again indicating a role for ANXA1 in the formation/stabilization of the actin cytoskeleton and cell polarity. To confirm that these changes in hCMEC/D3 cells are representative of the situation in vivo, we examined the F-actin cytoskeleton of primary cerebral capillaries from WT and AnxA1$^{-/-}$ mice, showing WT vessels to possess dense bundles of longitudinally aligned actin fibers, in marked contrast to AnxA1$^{-/-}$ vessels, in which only sparse actin fibers were evident (Fig. 3*D*).

In Vivo and in Vitro Rescue Effects of Recombinant ANXA1. We have previously reported an autocrine/paracrine activity of ANXA1 in the control of pituitary adrenocorticotropin release (14) and in the blockade of monocyte migration across the inflamed peripheral endothelium (15). Consequently, we investigated whether a similar action of ANXA1 could be identified in the restoration of BBB function in vivo and in vitro. i.v. administration of 0.67 μg/kg body weight (16) human recombinant ANXA1 (hrANXA1) to AnxA1$^{-/-}$ mice 24 h before the administration of Evans blue dye significantly reduced the degree of tracer extravasation into the brain, effectively rescuing the AnxA1$^{-/-}$ phenotype of enhanced BBB leakage (Fig. 4*A*). This phenomenon could be mimicked by the treatment of AnxA1$^{-/-}$ mouse brain microvascular endothelial primary cultures or AS hCMEC/D3 clones with hrANXA1 at 20 μg/mL, in which the protein was able to significantly reduce paracellular permeability toward that of control cells (Fig. 4 *B* and *C*) and to restore more normal actin organization (Fig. 4*D*), closely correlating with our in vivo data.

To further investigate the mechanism whereby recombinant ANXA1 could rescue the permeability deficit seen in AnxA1$^{-/-}$ mice or in AS clones, we analyzed the role of FPR2, which we have previously shown to mediate the actions of ANXA1 in different cellular contexts (14, 17, 18). By using flow cytometry, we confirmed the presence of FPR2 on the surface of hCMEC/D3 cells (Fig. 4*E*). Infection of hCMEC/D3 cells with lentiviral shRNA targeting FPR2 significant down-regulated surface FPR2 expression (Fig. 4*E*), leading to a basal increase in paracellular permeability, suggestive of an autocrine/paracrine action of endogenous ANXA1; and a complete abrogation of the response to exogenous ANXA1 (Fig. 4*F*). These findings were further confirmed by administration of WRW_4, a specific antagonist for FPR2 (19), which completely prevented the decrease in paracellular permeability induced by ANXA1 treatment (Fig. 4*G*), confirming that exogenous ANXA1 acts through FPR2. Furthermore, treatment of hCMEC/D3 cells with 20 μg/mL hrANXA1 induced a significant up-regulation in the proportion of occludin, VE-cadherin (Fig. 4*H*), ZO-1, and claudin-5 (Fig. S5) associated with the plasma membrane, supporting our hypothesis that ANXA1 affects tight junction expression and organization.

Following the identification of endogenous ANXA1 as a stabilizer for fibrillar actin and consequently cell polarity, we assessed the distribution of F-actin fibers or fibrils in WT and AS hCMEC/D3 cells following treatment with hrANXA1. Notably, AS cells exhibited a clear lack of transcellular F-actin fibrils along with a loss of lateral cellular polarity. However, treatment of the cells for 24 h with 20 μg/mL hrANXA1 restored a normal cellular polarity and induced the appearance of clear transcellular F-actin fibrils (Fig. 5*A*). These microscopic data were confirmed by biochemical analysis of the F/G actin ratio in the hCMEC/D3 cells treated with 20 μg/mL hrANXA1 or not treated, with an increase in actin polymerization being apparent within 3 h of treatment (Fig. 5*B*).

As we have identified ANXA1 to enhance paracellular permeability through intracellular and extracellular actions, we sought to identify the mechanism whereby the two pathways could be reconciled. Treatment of WT hCMEC/D3 cells for 3 h or 24 h with 20 μg/mL hrANXA1 induced a marked increase in intracellular ANXA1 (Fig. 6*A*), a result supported by previous studies identifying a similar effect of bioactive ANXA1 N-terminal peptide fragments upon total intracellular ANXA1 (20).

However, this self–up-regulating action of ANXA1 is not sufficient to explain the rescue effect upon BBB integrity seen following treatment of ANXA1-null mice with hrANXA1. To explain this phenomenon, we investigated the signaling pathways activated following binding of ANXA1 to FPR2. As heterotrimeric G proteins have been implicated in the control and regulation of the actin cytoskeleton and the maintenance of tight junction formation (21),

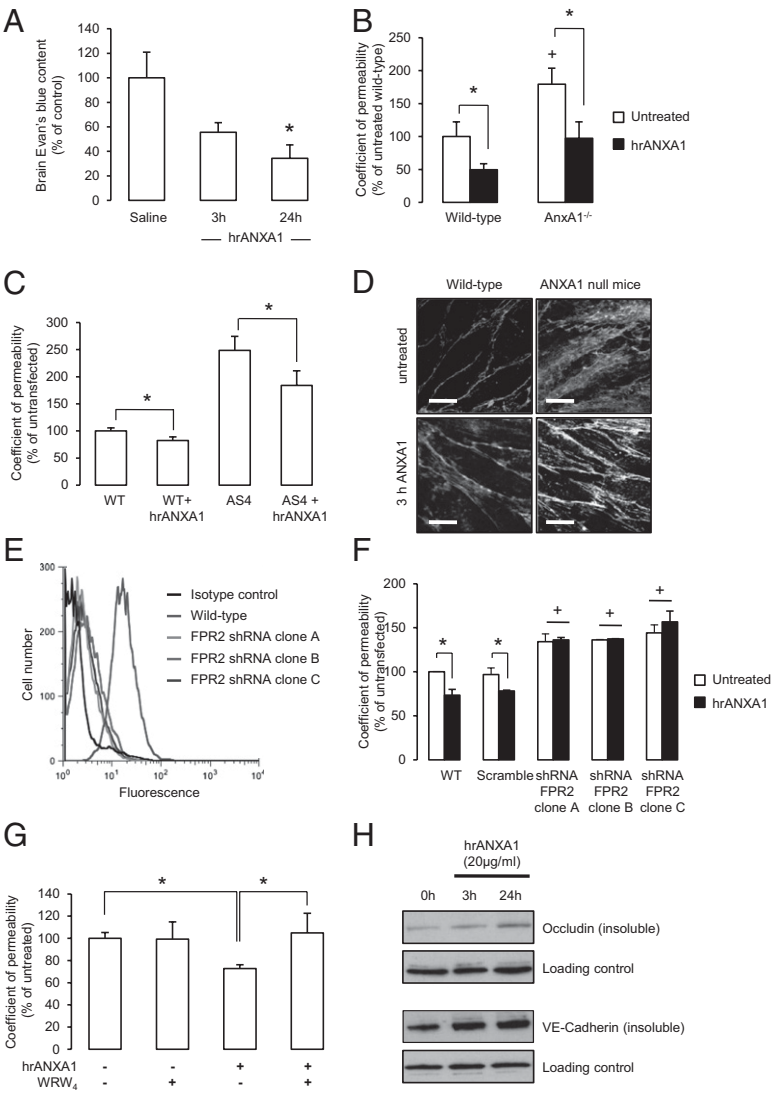

Fig. 4. Exogenous ANXA1 restores BBB integrity in vivo and in vitro. (*A*) AnxA1$^{-/-}$ mice ($n = 6$) were pretreated i.v. with 0.67 μg/kg body weight hrANXA1 in saline solution, and, after 3 h or 24 h, were further injected with 100 μL of 2% Evans blue in saline solution. Dye was allowed to circulate for 1 h before brain dye content was assessed spectrophotometrically and normalized to plasma levels (data are mean ± SEM; $^{*}P < 0.05$ vs. saline solution control). (*B*) Administration of 20 μg/mL hrANXA1 at 3 h before analysis of paracellular permeability significantly reduced permeability in primary brain endothelial cells isolated from AnxA1-null mice and littermate controls; data are representative of at least three independent experiments, performed in triplicate, expressed as mean ± SEM ($^{*}P < 0.05$, $^{+}P < 0.05$ vs. untreated WT). (*C*) Confocal microscopic analysis of monolayers of primary mouse brain capillary endothelial cells from WT and AnxA1$^{-/-}$ mice, grown under polarizing conditions on Transwell filters, showing rhodamine-phalloidin staining of F-actin in basal conditions and following treatment for 3 h with 20 μg/mL hrANXA1 (typical images from $n = 3$ independent preparations). (Scale bar: 10 μm.) (*D*) Administration of 20 μg/mL hrANXA1 3 h before analysis significantly reduced paracellular permeability in WT hCMEC/D3 cells, and significantly restored permeability in AS clones toward WT; data are representative of at least three independent experiments, performed in triplicate, expressed as mean ± SEM ($^{*}P < 0.05$). (*E*) Expression of FPR2 in untransfected hCMEC/D3 cells. Representative example of flow cytometric analysis of FPR2 expression in untransfected hCMEC/D3 cells; at least 10,000 events were analyzed; histograms represent one of six independent experiments. (*F*) Infection of hCMEC/D3 cells with shRNA targeting FPR2 (independent clones A–C), but not a scramble sequence, significantly enhances basal permeability and abolishes the decrease in permeability seen upon treatment with hrANXA1 (20 μg/mL, 3 h); data are representative of at least three independent experiments, performed in triplicate, expressed as mean ± SEM ($^{*}P < 0.05$, $^{+}P < 0.05$ vs. untreated WT cells). (*G*) Administration of the FPR2 antagonist WRW_4 at 5 μM 10 min before treatment with 20 μg/mL ANXA1 blocked the effect of ANXA1 on paracellular permeability; data are representative of at least three independent experiments, performed in triplicate, expressed as mean ± SEM ($^{*}P < 0.05$). (*H*) Administration of 20 μg/mL hrANXA1 to WT hCMEC/D3 cells induces an up-regulation of membrane-associated (i.e., insoluble) occludin and VE-cadherin expression as measured by Western blot. Data are representative of at least three independent experiments.

and we have already shown ANXA1 to regulate RhoA activity in endocrine cells (14), we measured RhoA-GTPase activity in the WT hCMEC/D3 cells and in ANXA1 antisense clones. Whereas levels of active RhoA were low in WT cells, activity was markedly increased in antisense clones (Fig. 6*B*). Importantly, this activity was significantly reduced by treatment with hrANXA1, indicating that the absence of endogenous ANXA1 permits excessive activity of RhoA, a factor known to signal for enhanced paracellular permeability via increased actin cytoskeleton instability (21). Thus, treatment of ANXA1 antisense hCMEC/D3 clones with hrANXA1 limits RhoA activity and stabilizes the actin cytoskeleton, enhancing the formation of tight junctions and ensuring appropriate BBB integrity.

Expression of ANXA1 Is Selectively Lost from Cerebral Capillaries in Patients with MS, but Not with Other Neurodegenerative Conditions. As progressive breakdown of the BBB has been documented in many major neurological disorders, including MS, Parkinson disease, and Alzheimer's disease (22), we examined the potential role of ANXA1 in these conditions (Table S1). Through immunofluorescent colocalization with the endothelial marker protein CD31, we first confirmed the presence of ANXA1 in the cerebral microvasculature of neurological disease-free postmortem human samples (Fig. 7*A*, representative of all patients examined). However, although examination of samples from patients with Parkinson disease revealed that expression of ANXA1 was maintained within the cerebral capillaries, ANXA1 was not detectable in those patients (Table S2) who had died with MS (Fig. 7*B*, representative of all patients examined). The loss of ANXA1 was moreover highly cell-specific, being limited to capillary endothelial cells of the BBB brain parenchyma, as leukocytes and other sites of brain ANXA1 expression, such as the ependyma, choroid plexus, and meningeal vessels, remained highly immunoreactive (Fig. 7*C*). Intriguingly, this was paralleled by a significant reduction in circulating ANXA1 in the plasma of patients with MS but not in age- and sex-matched healthy donors (Fig. 7*D* and Table S2). To examine the consequences of these two disease-related phenomena, we studied the effect of plasma from patients with MS upon BBB permeability by using the in vitro hCMEC/D3 model. Exposure to plasma from patients with MS induced a significant increase in transendothelial paracellular permeability, a finding closely correlating with a plasma-induced reduction in endothelial ANXA1 expression (Fig. 7*E*), and an effect moreover not seen in cells exposed to plasma from healthy donors. Furthermore, addition of hrANXA1 to plasma from patients with MS limited the increase in paracellular permeability seen upon exposure of hCMEC/D3 cells to the plasma (Fig. 7*F*). These data, together with the studies of the molecular and cellular actions of ANXA1 in the maintenance of BBB integrity, strongly indicate a significant role for ANXA1 in

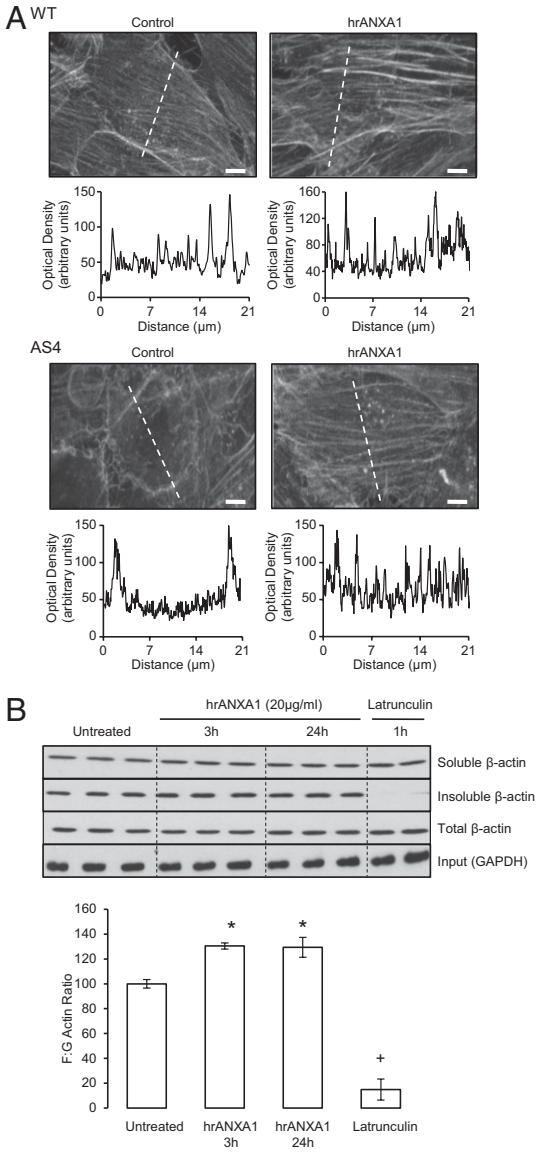

Fig. 5. Administration of exogenous ANXA1 induces F-actin formation. (*A*) Rhodamine-phalloidin staining of F-actin in untreated WT and AS4 hCMEC/D3 clones or clones treated for 3 h with 20 μg/mL hrANXA1. This treatment is shown to restore the abnormal cytoskeletal morphology seen in AS4 clones. (Scale bar: 10 μm.) Histograms represent intensity profiles of β-actin staining along the dotted lines in photomicrographs, emphasizing the differences in cross-cellular actin expression. (*B*) Biochemical analysis of G (soluble) and F (insoluble) β-actin in hCMEC/D3 cells treated with 20 μg/mL hrANXA1 for 3 h or 24 h, or with 10 μM of the actin-depolymerizing agent latrunculin (Sigma-Aldrich) for 1 h. Histograms represent analysis of three different experiments, performed in triplicate; data are mean ± SEM (*$P < 0.05$ vs. untreated, $^{+}P < 0.05$ vs. 3 h and 24 h treated samples and untreated).

BBB function, and highlight potential new avenues for therapeutic application in MS.

Discussion

The indispensible role of tight junctions in maintaining the integrity of the BBB, and their disruption in neurological diseases such as MS, suggest that therapies targeted to components of the tight junction complex or its regulatory factors hold significant promise for the treatment and prevention of disease. Our in vivo data show that BBB permeability is significantly greater in AnxA1$^{-/-}$ mice than in WT controls, a permeability defect that could be reversed by 24 h of treatment with hrANXA1. Complementary evidence obtained from the human brain microvascular endothelial cell line hCMEC/D3 showed ANXA1 expression to correlate with expression of tight junction proteins and, most importantly, with the stability of the actin cytoskeleton, regulating cellular polarity and consequent tight and adherens junction formation. Together, this work places ANXA1 at the center of the systems regulating BBB permeability, and highlights its role in the physiology of the cerebral microvasculature.

We have identified a number of pathways through which ANXA1 can regulate the cytoskeleton, principally through its interactions with β-actin. Among these is the direct binding of ANXA1 and β-actin, which, intriguingly, appears mainly, but not exclusively, to involve cytosolic rather than fibrillar actin. Given that ANXA1 appears to bind predominantly to soluble G-actin, it is tempting to speculate on a potential role for the protein in the stabilization of actin oligomers before addition to the growing cytoskeleton (23), an idea supported by the accumulation of points of ANXA1 and β-actin colocalization alongside F-actin fibers, and previous work showing ANXA1 to limit the inhibitory actions of profilin upon actin fiber elongation (24, 25). Additionally, we have identified an autocrine/paracrine action of ANXA1 signaling via FPR2 to inhibit the activity of the small GTPase RhoA. As RhoA is known to initiate a signaling pathway resulting in the destabilization of the actin cytoskeleton, ultimately enhancing paracellular permeability (21), such an effect of exogenous ANXA1 will significantly help in maintaining BBB integrity. We propose that these two pathways act in concert to maintain tight junction formation, and, through this, preserve efficient BBB function (Fig. 8).

This second effect of ANXA1 may be particularly important from a pharmacological point of view, as it highlights the importance of the G protein-coupled receptor FPR2 in the maintenance of BBB structure and function, and suggests it may well be amenable to future therapeutic targeting in conditions associated with an impaired BBB, such as MS. This point is further reinforced by our experiments (*i*) with the AnxA1-null mouse, in which, even in the absence of intracellular AnxA1, we could induce a significant phenotypic rescue through treatment with hrANXA1; and (*ii*) in vitro, in which knock-down of FPR2 expression prevented the restorative effects of ANXA1, again highlighting the central role of FPR2 and its potential for therapeutic exploitation.

Our finding of a selective loss of ANXA1 expression in the cerebral capillary endothelium of patients with MS is particularly important, as it may go a long way in understanding the cause of the deficits in BBB permeability seen in this disease (26). In particular, disrupted occludin expression and distribution have been reported within the microvascular endothelium of patients with MS (27), clearly paralleling our findings in AnxA1$^{-/-}$ mice and AS hCMEC/D3 clones. It is important to note that endothelial ANXA1 down-regulation occurs in normal-appearing white matter, a finding that may inform the extensive discussion whether deficits in BBB permeability precede leukocyte extravasation or are a consequence of immune cell accumulation (28). In particular, our finding that ANXA1 down-regulation occurs at sites distant from active lesions strongly suggests a preexisting weakening of BBB integrity before leukocyte extravasation and the development of active demyelination.

Previous reports have suggested beneficial (29) and detrimental (30) roles for ANXA1 in the widely used animal model of MS, experimental autoimmune encephalitis, a confusion heightened by evidence suggesting the expression of ANXA1 in disease plaques in MS (31). Several reasons may underlie the lack of clarity over the role of ANXA1 identified by these studies, and the discrepancy with some of our findings from human disease, not least of which is the use of an animal model itself (32); however, it is important to note that we have studied the role of ANXA1 in a defined cell/tissue type and the contribution the protein makes to the maintenance of BBB integrity, rather than examining the

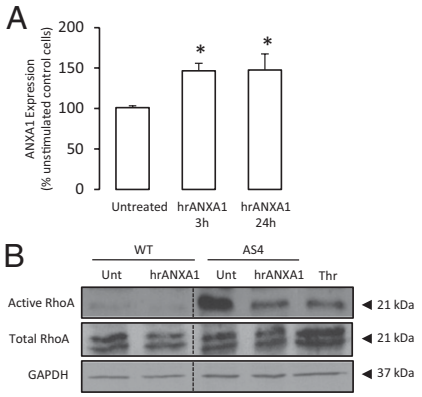

Fig. 6. Exogenous ANXA1 enhances endogenous ANXA1 and inhibits activity of the RhoA small GTPase in hCMEC/D3 cells. (*A*) Treatment of WT hCMEC/D3 cells with 20 μg/mL hrANXA1 for 3 h or 24 h induces an up-regulation in endogenous ANXA1 expression; data are representative of at least three different experiments, performed in triplicate, and are mean ± SEM (*$P < 0.05$ vs. untreated cells). (*B*) hCMEC/D3 cells transfected with an antisense sequence to ANXA1 exhibit constitutively increased activity of the small GTPase RhoA, an effect that can be reversed by treatment with 20 μg/mL hrANXA1 for 3 h. Thrombin (Thr; used at 1 IU/mL in serum-free medium for 8 min) was used as a positive control. Data are representative of at least three independent experiments.

multiple complex interacting systems that may be involved in a whole animal model of disease.

ANXA1 is well known as a mediator of glucocorticoid action in many body systems (33). In particular, we have previously shown glucocorticoids to limit leukocyte extravasation through the induction of ANXA1 release, whereupon ANXA1 binds to the $\alpha_4\beta_1$ integrin VLA_4, blocking leukocyte adhesion to the endothelium (15). Although studies have focused on leukocyte-derived ANXA1 binding to $\alpha_4\beta_1$ integrin, the endothelium may also serve as a source of circulating ANXA1, constitutively limiting leukocyte adhesion. As cerebral microvascular endothelial ANXA1 is down-regulated in MS, this may permit excessive leukocyte adhesion, and impair the ability of the BBB to prevent immune cell extravasation, a point reinforced by the use of natalizumab as a therapeutic strategy for this disease (34), given that the target of this monoclonal antibody therapy is the same $\alpha_4\beta_1$ integrin targeted by ANXA1. Moreover, glucocorticoids are themselves used as therapeutic agents in the treatment of MS (6), and the up-regulation of ANXA1 we have previously shown to occur following their administration (5) may underlie at least part of their therapeutic effect, restoring BBB function and correcting regulation of the brain parenchymal microenvironment. Importantly, our data further suggest a potential pharmacological role for ANXA1 itself in the treatment of BBB failure, as in vivo and in vitro studies revealed the ability of exogenous protein to restore BBB integrity, acting through FPR2 and modulating actin polymerization (Fig. 8), as we have previously reported (14).

A question remains why ANXA1 appears to be selectively down-regulated in the BBB endothelium in MS, but not in conditions such as Parkinson or Alzheimer's diseases, which are also associated with a degree of BBB breakdown (35, 36). At present, the reasons for this difference are unclear, but may reflect a brain-intrinsic source of degeneration and inflammation in Parkinson and Alzheimer's disease, as opposed to the inappropriate activation of the peripheral immune system seen in the autoimmune disease MS. This idea is indirectly supported by independent previous reports indicating that serum from patients with MS can decrease transendothelial resistance in vitro (37), and that such serum can induce a down-regulation in ANXA1 among other proteins (38). Our data confirm and extend these two studies, not only providing a clear rationale for a correlation between ANXA1 expression and changes in BBB permeability in MS, but also revealing a potential therapeutic strategy aimed at reversing the defect in BBB function seen in MS.

Together, our findings may have important consequences for our understanding of the BBB response to inflammation, as exposure to proinflammatory cytokines, e.g., TNF-α and IFN-γ, has been shown to disrupt the BBB endothelium via RhoA (39) and PLA_2-dependent pathways (40). As we and others have shown ANXA1 to inhibit $sPLA_2$ and $cPLA_2$ activity (10, 41), and our present and previous work suggests ANXA1 interacts with RhoA (18), it is plausible to suggest that ANXA1 may well be able to limit inflammation-associated BBB breakdown. If confirmed, this would represent a novel neuroprotective mechanism of action of ANXA1 and could thus have high potential utility in the treatment of BBB disruption.

Much exciting progress has been, and is being made, in understanding the molecular basis of BBB structure and function, and, although some details remain obscure, the tight junction appears to be at the convergence of multiple cellular signaling pathways regulating paracellular permeability. Our finding of a central role for the endogenous protein ANXA1 in these processes, and, more importantly, the potential for exogenous administration of this protein to rescue defects in BBB function, highlight the importance of studying endogenous mediators to provide new indicators for therapeutic approaches, with promise for the treatment of severe CNS diseases such as MS.

Methods

Human Tissue. Human postmortem samples were taken from the prefrontal cortex of cases of neuropathologically confirmed MS and Parkinson disease cases and from nonneurologic controls; brains were retrieved from the UK Multiple Sclerosis Society and UK Parkinson Disease Society tissue banks at Imperial College London. Brains were selected according to the following criteria: (*i*) availability of full clinical history, (*ii*) no evidence of cancer postmortem, and (*iii*) negligible atherosclerosis of cerebral vasculature. Demographic data for the samples used are described in Table S1. Tissue was fixed in 10% (vol/vol) buffered formalin and embedded in paraffin. From each paraffin block, 8-μm sections were cut and used for immunohistochemistry as described later. Human plasma samples from patients with MS and healthy donors were used to measure ANXA1 content by ELISA as reported previously (18).

Animal Experiments. Four-month-old male C57BL/6 WT or $ANXA1^{-/-}$ mice (42) were bred in house, with all $ANXA1^{-/-}$ mice being genotyped by PCR before use. BBB permeability was assessed in vivo by administration of Evans blue dye as described previously (43). In some experiments, hrANXA1 was administered i.v. at 0.67 μg/kg body weight as previously described (16) before Evans blue dye injection.

MRI. MRI of anesthetized WT and AnxA1-null mice was performed by using a 9.4-T Varian Direct Drive system and quadrature volume head RF coil. The MRI protocol consisted of dynamic contrast acquisitions with a multislice T1-weighted gradient echo with a fixed 30° flip angle (repetition time, 132 ms; echo time, 2.77 ms; field of view, 20 × 20 mm; matrix size, 128 × 96, 24 contiguous transverse slices of 0.6 mm covering the whole brain). A total of 50 volumes were acquired, with 100 μL of 0.5 mM dimeglumine gadopentetate (Magnevist; Schering) administered directly after the 14th volume at a rate of 3.3 μL/s. TOPPCAT software* was used to create quantitative maps of fractional blood volume.

hCMEC/D3 Cells. The immortalized human brain microvascular endothelial cell line, hCMEC/D3, was cultured in tissue culture flasks coated for 2 h at 37 °C in rat tail collagen type I solution as recommended by the manufacturer (BD Diagnostics) and in EBM-2 medium (Lonza) supplemented with VEGF (unless otherwise stated), IGF1, EGF, basic FGF, hydrocortisone, ascorbic acid,

*Barboriak DP, et al. International Society for Magnetic Resonance in Medicine Workshop on MR in Drug Development: From Discovery to Clinical Therapeutic Trials, April 2–3, 2004, McLean, VA.

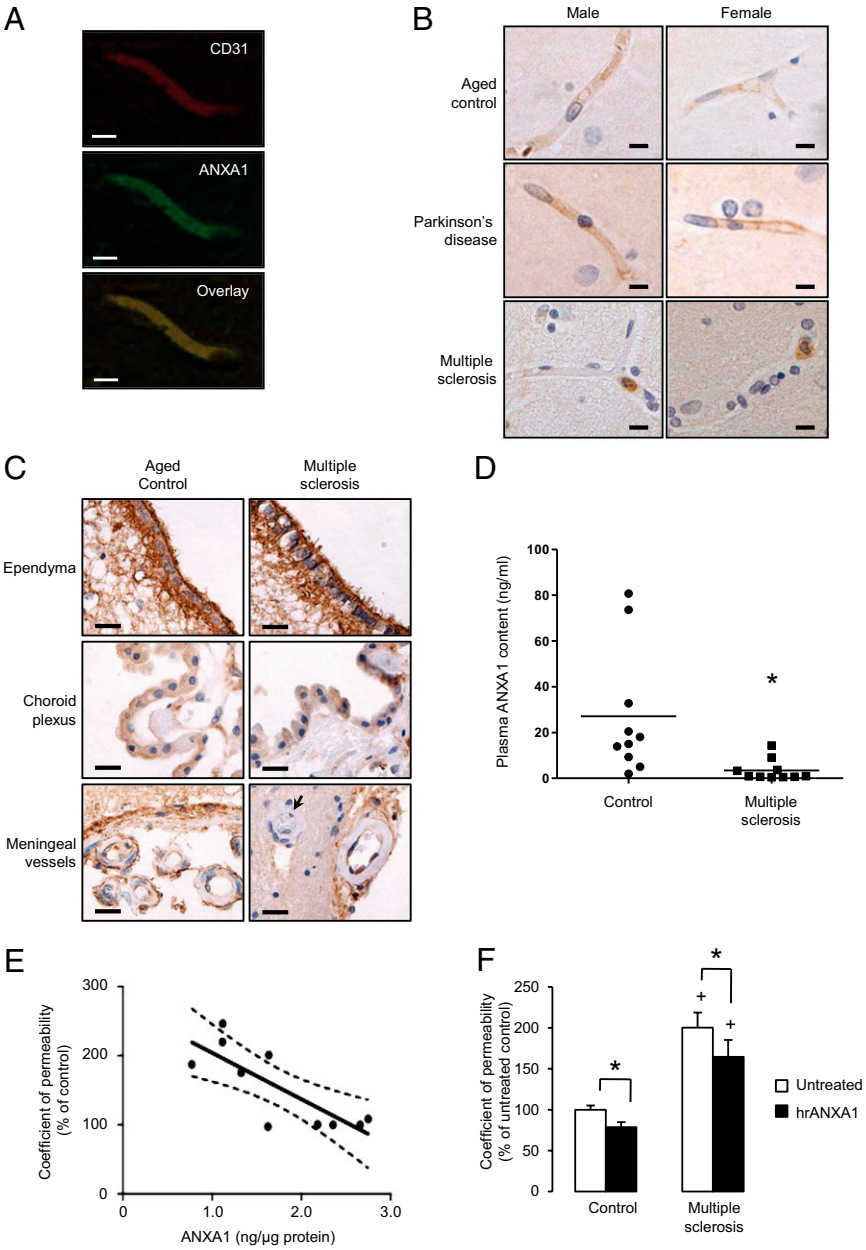

Fig. 7. Expression of ANXA1 is selectively lost from the cerebral capillaries of patients with MS, but not those with other neurodegenerative conditions. (*A*) Confocal microscopic analysis of ANXA1 expression within the endothelium of a typical human cortical capillary, immunofluorescently labeled for CD31 (green) and ANXA1 (red). (Scale bar: 10 μm.) (*B*) Representative immunohistochemical analysis of ANXA1 expression within cortical capillaries of human male and female postmortem brains. Note in particular the strong expression of ANXA1 in circulating leukocytes of patients with MS, but the absence of endothelial ANXA1 immunostaining (typical images from cases described in Table S1; sections are 8 μm thick). (Scale bar: 10 μm.) (*C*) Immunohistochemical analysis of ANXA1 expression within the ependyma of the lateral ventricles, the choroid plexus, and the meningeal blood vessels of aged control subjects and patients with MS. Note in particular the expression of ANXA1 in meningeal vessel endothelial cells, but not parenchymal vessel endothelial cells (arrow) in patients with MS (sections are 8 μm thick). (Scale bar: 20 μm.) (*D*) Plasma ANXA1 content from patients with MS and healthy age- and sex-matched control subjects (lines indicate mean values; $*P < 0.05$, Student *t* test). (*E*) Paracellular permeability coefficient (expressed as percentage of the untreated control) of monolayers of human hCMEC/D3 cells following exposure for 24 h to medium containing 20% plasma from patients with MS, correlated with total levels of ANXA1 in the same hCMEC/D3 cells following exposure (linear regression line and 95% CIs are marked; coefficient of correlation is −0.797; $P < 0.01$). (*F*) Administration of exogenous hrANXA1 to plasma from patients with MS limits the increase in permeability caused upon application of the plasma to WT hCMEC/D3 cells (24 h exposure to 20% MS plasma in normal medium); data are representative of three independent experiments, using serum from at least 10 different patients with MS, performed in triplicate, and expressed as mean ± SEM ($*P < 0.05$, $^{+}P < 0.05$ vs. control).

gentamycin, and 2.5% (vol/vol) FBS as provided and recommended by the manufacturer, giving microvascular endothelial cell medium-2. Cultures were maintained at 37 °C in 5% CO_2, replaced with fresh medium every 3 d, and split when they reached 70% confluence.

Stable hCMEC/D3 cell lines were produced by transfection with an empty pRc/CMV plasmid or constructs bearing the full length or an antisense sequence for human ANXA1 (10) using HiFect according to manufacturer instructions (Lonza). Cells were screened for analysis of ANXA1 expression by flow cytometry and for expression of the neomycin resistance cassette by RT-PCR according to standard protocols (44).

Primary Cerebral Capillary Isolation and Culture. Capillaries were extracted from the cortex of 4-mo-old WT or AnxA1-null mice according to published protocols (43). Isolated vessels were put in culture for further analysis (e.g., paracellular permeability) or fixed in 2% (wt/vol) PFA for 15 min, washed twice in 0.05 M PBS solution, and immunostained as described earlier for cell line-based analyses.

Permeability Studies. hCMEC/D3 cells were grown on Transwell polycarbonate filters (pore size, 0.4 μm; Sigma-Aldrich) first coated with calf skin collagen type I (Sigma-Aldrich) and bovine plasma fibronectin (Sigma-Aldrich). Paracellular permeability of 70-kDa FITC-dextran was assessed after stimulation as previously described (11); transendothelial resistance across the monolayer was determined by using an Endohmeter (World Precision Instruments). Resistance from coated cell-free inserts was always subtracted from the resistance obtained in the presence of endothelial cells.

Immunohistochemistry. Immunohistochemical analysis of human and murine tissues and hCMEC/D3 cells was performed according to standard procedures by using primary antibodies directed against ANXA1 (1:1,000; Invitrogen), CD31 (1:300; DAKO), occludin (1:300; Invitrogen), claudin-5 (1:300; Invitrogen), β-actin (1:500; Abcam), VE-cadherin (1:250; eBioscience), zonula occludens-1 (ZO-1; 1:100; Invitrogen), PDGF receptor (1:1,000; Invitrogen), GFAP (1:500; DAKO), α-laminin (1:500; Invitrogen), and perlecan (1:500; Invitrogen). Secondary antibodies were horseradish peroxidase-conjugated goat anti-rabbit IgG (1:500; Vector Laboratories) or Alexa Fluor 488- or 594-conjugated goat anti-rabbit or anti-mouse IgG (1:500; Invitrogen). Samples were counterstained with DAPI, and certain hCMEC/D3 samples were stained with rhodamine-conjugated phalloidin (5 μg/mL; Invitrogen). Proximity ligation assays (Duolink; Olink Bioscience) between ANXA1 and β-actin were performed on

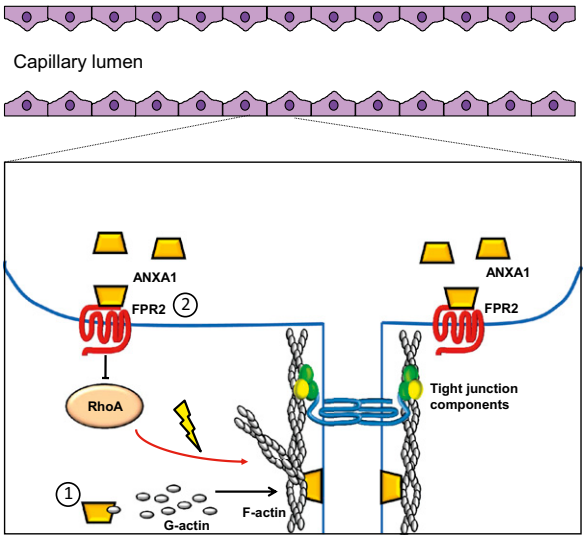

Fig. 8. Schematic representations of potential mechanisms of action of ANXA1 in maintaining BBB integrity. *1*, Endogenous ANXA1 binds to β-actin, promoting cytoskeleton formation, and serving as an anchor linking it to the plasma membrane facilitating the establishment of tight junctions between endothelial cells. *2*, Exogenous ANXA1 acting via FPR2 inhibits the activity of RhoA, promoting cytoskeletal stability and enhancing tight junction formation, hence contributing to BBB integrity.

hCMEC/D3 cells according to the manufacturer's instructions. Briefly, following blocking with proprietary blocking agent, samples were incubated overnight at 4 °C with a polyclonal rabbit anti-ANXA1 antibody (1:1,000; Invitrogen) and a monoclonal mouse anti–β-actin antibody (1:500; Abcam). All other steps were performed according to the manufacturer's instructions by using the reagents and media included in the proximity ligation assay kit. Following a final wash step, samples were counterstained with AF488-conjugated phalloidin (5 μg/mL; Invitrogen), and were visualized by using confocal microscopy as described in the following section.

Microscopy. Bright-field photomicrographs were captured at 22 °C by using a Nikon Eclipse E800 microscope fitted with a 60× oil immersion objective lens (NA, 1.4 mm; working distance, 0.21 mm), a CoolSNAP-Pro$_{cf}$ camera (Roper Scientific), and Image ProPlus 4.5.1 software (Perkin-Elmer). Fluorescent images were captured at 22 °C by using a TCS SP5 confocal laser scanning microscope (Leica Microsystems) fitted with 405-nm, 488-nm, 594-nm, and 633-nm lasers, and attached to a Leica DMI6000CS inverted microscope fitted with a 63× oil immersion objective lens (NA, 1.4 mm; working distance, 0.17 mm). Images were captured with Leica LAS AF 2.6.1 software and analyzed by using ImageJ software (National Institutes of Health). EM analysis of ANXA1 expression in hCMEC/D3 cells grown as a monolayer on Transwell filters was performed essentially as described previously (14). In brief, monolayers were fixed in 0.05% glutaraldehyde, 3% (wt/vol) formaldehyde in 0.1 M PBS solution, pH 7.4, before cryoprotection and embedding in LRGold acrylic resin (London Resin). Ultrathin (50–80 nm) transverse and longitudinal sections were stained for ANXA1 by Immunogold labeling by using a well-characterized sheep polyclonal anti-ANXA1 antiserum, and examined morphologically. Sections were examined with a model1010 transmission electron microscope (JEOL).

Flow Cytometry. hCMEC/D3 cells were immunophenotyped by flow cytometry following immunofluorescent staining as described earlier. Total vs. surface protein content was defined by the inclusion or omission of 0.025% saponin at all stages of the staining procedure. Cells were analyzed by using a FACScan II analyzer (Becton Dickinson) equipped with a 15-mW argon ion laser and CellQuest software (BD Biosciences); in all experiments, a minimum of 10,000 events were analyzed per profile.

Western Blot and Coimmunoprecipitation. For tight and adherens junctions analysis (ZO-1, occludin, claudin-5, VE-cadherin), cortical tissue samples from WT and ANXA1-null mice were separated by following a published protocol (45), which first involves rapid homogenization in lysis buffer A (2 mM EDTA, 10 mM EGTA, 0.4% NaF, 20 mM Tris·HCl, protease inhibitors, pH 7.4) to obtain the soluble protein fraction, and then disruption of the pellet by sonication with buffer A supplemented with 1% Triton X-100 and 0.2% SDS to obtain the insoluble membrane-associated protein fraction. Total samples (MDR-1, ANXA2, and ANXA5) were extracted by homogenization of tissue in RIPA buffer (1 mM EDTA, 150 mM NaCl, 50 mM Tris·HCl, 1% Triton X-100, 0.1% SDS, 1% sodium deoxycholate, protease inhibitors, pH 7.4). Soluble and insoluble β-actin fractions were extracted as reported previously (46). Blots were incubated overnight at 4 °C in antibodies raised against occludin (1:200; Invitrogen), claudin-5 (1:1,000; Santa Cruz), VE-cadherin (1:200; Santa Cruz), MDR1a (1:500; Santa Cruz), and β-actin (1:5,000; Abcam) chosen as a loading control, washed in TBS-Tween, and incubated for 1 h at room temperature with HRP-conjugated sheep anti-rabbit or sheep anti-mouse antisera (1:15,000; Serotec). Immunoreactive bands were detected by chemiluminescence using ECL reagents and brief exposure to Hyperfilm (all GE Healthcare). Blots were then scanned and analyzed with ImageJ software.

For coimmunoprecipitation experiments, total hCMEC/D3 extracts were prepared in RIPA buffer, and 250 μg of total protein extract was first precleared with mouse control serum (Sigma-Aldrich), incubated with anti-ANXA1 (5 μg per sample) or anti–β-actin (5 μg per sample) antibodies overnight at 4 °C and then with protein G-agarose–conjugated beads. The final pellet was resuspended in 10 mM Tris HCl, pH 7.4, supplemented with 1 mM PMSF and analyzed by Western blot.

RhoA Pulldown Assays. hCMEC/D3 cells were grown on 6-cm Petri dishes until confluence and then incubated overnight in complete microvascular endothelial cell medium-2 without VEGF before exposure to recombinant hANXA1. Cells were then lysed, and RhoA activity was measured with recombinant GST-Rhotekin bound to glutathione beads (gift from Beata Wojciak-Stothard, Imperial College London, London, United Kingdom) as previously reported (39), whereas the activity of Rac1 was measured with GST-p21–activated kinase binding domain (Cell Biolabs). Affinity-precipitated RhoA proteins were resolved by SDS/PAGE and detected by Western blotting.

shRNA FPR2 and Virus Production. MISSION shRNA bacterial glycerol stocks were purchased from Sigma-Aldrich. The MISSION shRNA clones used are sequence-verified shRNAs for FPR2, cloned in the pLKO.1 lentiviral vector (pLKO.1-puro) and provided as frozen bacterial glycerol stocks [Luria broth, carbenicillin at 100 μg/mL, and 10% (vol/vol) glycerol] for propagation and downstream purification of the shRNA clones. Specifically, the FPR2 targeting shRNAs sequences used were as follows: TRCN0000356999–FPR2 A, TRCN0000357000–FPR2 B, and TRCN0000378222–FPR2 C. High-titer lentiviral preparations in HEK293T cells and lentiviral infections were carried out as described previously (47). Briefly, HEK293T packaging cells were transfected by calcium phosphate with pLKO.1 and packaging vectors. Supernatants were harvested at 36 to 60 h; virions were concentrated by ultracentrifugation and stored at −80 °C. hCMEC/D3 endothelial cells were seeded in six-well plate at 70% confluence. The following day, virus was added directly to the medium of the cell culture in the presence of Polybrene (5 μg/mL). The plate was spun for 1 h at 1,300 × *g*, and cells were incubated at 37 °C for 48 h. Infected cells were allowed to expand and were prepared for paracellular permeability analyses. The transduction efficiency and FPR2 knockdown were verified by FACS analysis.

Statistical Analysis. All quantified data were tested for normality and analyzed by one- or two-way ANOVA as appropriate, with post hoc comparisons using the Tukey honestly significant difference procedure. In all cases, a P value ≤ 0.05 was taken as indicating statistical significance.

Ethical Approval. All animal experiments were performed in accordance with the UK Animals (Scientific Procedures) Act, 1986, following approval by the UK Home Office. Human tissue samples were provided by the UK Multiple Sclerosis Tissue Bank and the UK Parkinson's Disease Society Tissue Bank at Imperial College London. Patients' blood samples were provided by A. Malaspina (East London and the City Research Ethics Committee: 09/H0703/27). Informed consent was obtained from all those individuals recruited to the study. Blood samples and clinical information were collected following consent. The study followed established standard operating procedures, was approved by the East London & The City Local Research Ethics Committee, and the experiments conformed to the principles set out in the World Medical Association Declaration of Helsinki.

ACKNOWLEDGMENTS. We thank the UK Multiple Sclerosis Tissue Bank and the UK Parkinson's Disease Society Tissue Bank at Imperial College London for provision of human tissue samples under their ethical approval; Dr. Beata Wojciak-Stothard (Imperial College London) for providing the antibodies and beads for RhoA signaling analysis and for her help and advice;

Dr. Rachel Brown (King's College London) for helping in the isolation of mouse brain endothelial cells for primary culture; and Prof. Chris Reutelingsperger (University of Maastricht) for donating hrANXA1. This work was supported by Wellcome Trust Grants 085123 and 085983.

1. Abbott NJ, Patabendige AA, Dolman DE, Yusof SR, Begley DJ (2010) Structure and function of the blood-brain barrier. *Neurobiol Dis* 37(1):13–25.
2. Engelhardt B, Sorokin L (2009) The blood-brain and the blood-cerebrospinal fluid barriers: Function and dysfunction. *Semin Immunopathol* 31(4):497–511.
3. Yona S, et al. (2006) Impaired phagocytic mechanism in annexin 1 null macrophages. *Br J Pharmacol* 148(4):469–477.
4. Solito E, et al. (2008) Annexin A1 in the brain—undiscovered roles? *Trends Pharmacol Sci* 29(3):135–142.
5. Go KG, et al. (1994) Effect of steroids on brain lipocortin immunoreactivity. *Acta Neurochir Suppl (Wien)* 60:101–103.
6. de Boer AG, Gaillard PJ (2006) Blood-brain barrier dysfunction and recovery. *J Neural Transm* 113(4):455–462.
7. Moss SE, Morgan RO (2004) The annexins. *Genome Biol* 5(4):219.
8. Weksler BB, et al. (2005) Blood-brain barrier-specific properties of a human adult brain endothelial cell line. *FASEB J* 19(13):1872–1874.
9. Cucullo L, et al. (2008) Immortalized human brain endothelial cells and flow-based vascular modeling: A marriage of convenience for rational neurovascular studies. *J Cereb Blood Flow Metab* 28(2):312–328.
10. Solito E, Raguenes-Nicol C, de Coupade C, Bisagni-Faure A, Russo-Marie F (1998) U937 cells deprived of endogenous annexin 1 demonstrate an increased PLA_2 activity. *Br J Pharmacol* 124(8):1675–1683.
11. Dehouck MP, et al. (1992) Drug transfer across the blood-brain barrier: Correlation between in vitro and in vivo models. *J Neurochem* 58(5):1790–1797.
12. Wittchen ES, Haskins J, Stevenson BR (1999) Protein interactions at the tight junction. Actin has multiple binding partners, and ZO-1 forms independent complexes with ZO-2 and ZO-3. *J Biol Chem* 274(49):35179–35185.
13. Lundberg M, Eriksson A, Tran B, Assarsson E, Fredriksson S (2011) Homogeneous antibody-based proximity extension assays provide sensitive and specific detection of low-abundant proteins in human blood. *Nucleic Acids Res* 39(15):e102.
14. McArthur S, et al. (2009) Annexin A1 regulates hormone exocytosis through a mechanism involving actin reorganization. *FASEB J* 23(11):4000–4010.
15. Solito E, Romero IA, Marullo S, Russo-Marie F, Weksler BB (2000) Annexin 1 binds to U937 monocytic cells and inhibits their adhesion to microvascular endothelium: Involvement of the alpha 4 beta 1 integrin. *J Immunol* 165(3):1573–1581.
16. de Coupade C, Ajuebor MN, Russo-Marie F, Perretti M, Solito E (2001) Cytokine modulation of liver annexin 1 expression during experimental endotoxemia. *Am J Pathol* 159(4):1435–1443.
17. Perretti M, et al. (2002) Endogenous lipid- and peptide-derived anti-inflammatory pathways generated with glucocorticoid and aspirin treatment activate the lipoxin A4 receptor. *Nat Med* 8(11):1296–1302.
18. McArthur S, et al. (2010) Annexin A1: A central player in the anti-inflammatory and neuroprotective role of microglia. *J Immunol* 185(10):6317–6328.
19. Stenfeldt AL, et al. (2007) Cyclosporin H, Boc-MLF and Boc-FLFLF are antagonists that preferentially inhibit activity triggered through the formyl peptide receptor. *Inflammation* 30(6):224–229.
20. Rescher U, Danielczyk A, Markoff A, Gerke V (2002) Functional activation of the formyl peptide receptor by a new endogenous ligand in human lung A549 cells. *J Immunol* 169(3):1500–1504.
21. Terry S, Nie M, Matter K, Balda MS (2010) Rho signaling and tight junction functions. *Physiology (Bethesda)* 25(1):16–26.
22. Zlokovic BV (2008) The blood-brain barrier in health and chronic neurodegenerative disorders. *Neuron* 57(2):178–201.
23. Dominguez R (2010) Structural insights into de novo actin polymerization. *Curr Opin Struct Biol* 20(2):217–225.
24. Alvarez-Martinez MT, et al. (1996) Characterization of the interaction between annexin I and profilin. *Eur J Biochem* 238(3):777–784.
25. Alvarez-Martinez MT, Porte F, Liautard JP, Sri Widada J (1997) Effects of profilin-annexin I association on some properties of both profilin and annexin I: Modification of the inhibitory activity of profilin on actin polymerization and inhibition of the self-association of annexin I and its interactions with liposomes. *Biochim Biophys Acta* 1339(2):331–340.
26. Alvarez JI, Cayrol R, Prat A (2011) Disruption of central nervous system barriers in multiple sclerosis. *Biochim Biophys Acta* 1812(2):252–264.
27. Plumb J, McQuaid S, Mirakhur M, Kirk J (2002) Abnormal endothelial tight junctions in active lesions and normal-appearing white matter in multiple sclerosis. *Brain Pathol* 12(2):154–169.
28. Larochelle C, Alvarez JI, Prat A (2011) How do immune cells overcome the blood-brain barrier in multiple sclerosis? *FEBS Lett* 585(23):3770–3780.
29. Huitinga I, et al. (1998) Effect of annexin-1 on experimental autoimmune encephalomyelitis (EAE) in the rat. *Clin Exp Immunol* 111(1):198–204.
30. Paschalidis N, et al. (2009) Modulation of experimental autoimmune encephalomyelitis by endogenous annexin A1. *J Neuroinflammation* 6:33.
31. Probst-Cousin S, et al. (2002) Expression of annexin-1 in multiple sclerosis plaques. *Neuropathol Appl Neurobiol* 28(4):292–300.
32. Friese MA, et al. (2006) The value of animal models for drug development in multiple sclerosis. *Brain* 129(Pt 8):1940–1952.
33. Solito E, Nuti S, Parente L (1994) Dexamethasone-induced translocation of lipocortin (annexin) 1 to the cell membrane of U-937 cells. *Br J Pharmacol* 112(2):347–348.
34. Engelhardt B, Kappos L (2008) Natalizumab: Targeting alpha4-integrins in multiple sclerosis. *Neurodegener Dis* 5(1):16–22.
35. Kortekaas R, et al. (2005) Blood-brain barrier dysfunction in parkinsonian midbrain in vivo. *Ann Neurol* 57(2):176–179.
36. Zipser BD, et al. (2007) Microvascular injury and blood-brain barrier leakage in Alzheimer's disease. *Neurobiol Aging* 28(7):977–986.
37. Proia P, et al. (2009) Neuronal and BBB damage induced by sera from patients with secondary progressive multiple sclerosis. *Int J Mol Med* 24(6):743–747.
38. Alexander JS, et al. (2007) Proteomic analysis of human cerebral endothelial cells activated by multiple sclerosis serum and IFNbeta-1b. *J Mol Neurosci* 32(3):169–178.
39. Wojciak-Stothard B, Tsang LY, Paleolog E, Hall SM, Haworth SG (2006) Rac1 and RhoA as regulators of endothelial phenotype and barrier function in hypoxia-induced neonatal pulmonary hypertension. *Am J Physiol Lung Cell Mol Physiol* 290(6):L1173–L1182.
40. Heller RA, Krönke M (1994) Tumor necrosis factor receptor-mediated signaling pathways. *J Cell Biol* 126(1):5–9.
41. Parente L, Solito E (2004) Annexin 1: More than an anti-phospholipase protein. *Inflamm Res* 53(4):125–132.
42. Hannon R, et al. (2003) Aberrant inflammation and resistance to glucocorticoids in annexin 1-/- mouse. *FASEB J* 17(2):253–255.
43. Coisne C, et al. (2005) Mouse syngenic in vitro blood-brain barrier model: A new tool to examine inflammatory events in cerebral endothelium. *Lab Invest* 85(6):734–746.
44. Solito E, et al. (2006) Post-translational modification plays an essential role in the translocation of annexin A1 from the cytoplasm to the cell surface. *FASEB J* 20(9):1498–1500.
45. Liu LB, Xue YX, Liu YH, Wang YB (2008) Bradykinin increases blood-tumor barrier permeability by down-regulating the expression levels of ZO-1, occludin, and claudin-5 and rearranging actin cytoskeleton. *J Neurosci Res* 86(5):1153–1168.
46. Cramer LP, Briggs LJ, Dawe HR (2002) Use of fluorescently labelled deoxyribonuclease I to spatially measure G-actin levels in migrating and non-migrating cells. *Cell Motil Cytoskeleton* 51(1):27–38.
47. Rubinson DA, et al. (2003) A lentivirus-based system to functionally silence genes in primary mammalian cells, stem cells and transgenic mice by RNA interference. *Nat Genet* 33(3):401–406, and errata (2003) 34(2):231 and (2007) 39(6):803.